

Applicability of post-ionization theory to laser-assisted field evaporation of magnetite

D. K. Schreiber, A. N. Chiamonti, L. M. Gordon, and K. Kruska

Citation: [Applied Physics Letters](#) **105**, 244106 (2014); doi: 10.1063/1.4904802

View online: <http://dx.doi.org/10.1063/1.4904802>

View Table of Contents: <http://scitation.aip.org/content/aip/journal/apl/105/24?ver=pdfcov>

Published by the [AIP Publishing](#)

Articles you may be interested in

[Evidence of lateral heat transfer during laser assisted atom probe tomography analysis of large band gap materials](#)

Appl. Phys. Lett. **99**, 084101 (2011); 10.1063/1.3622647

[Field evaporation mechanism of bulk oxides under ultra fast laser illumination](#)

J. Appl. Phys. **110**, 044321 (2011); 10.1063/1.3610523

[Resolution of the transfer direction of field-evaporated gold atoms for nanofabrication and microelectromechanical system applications](#)

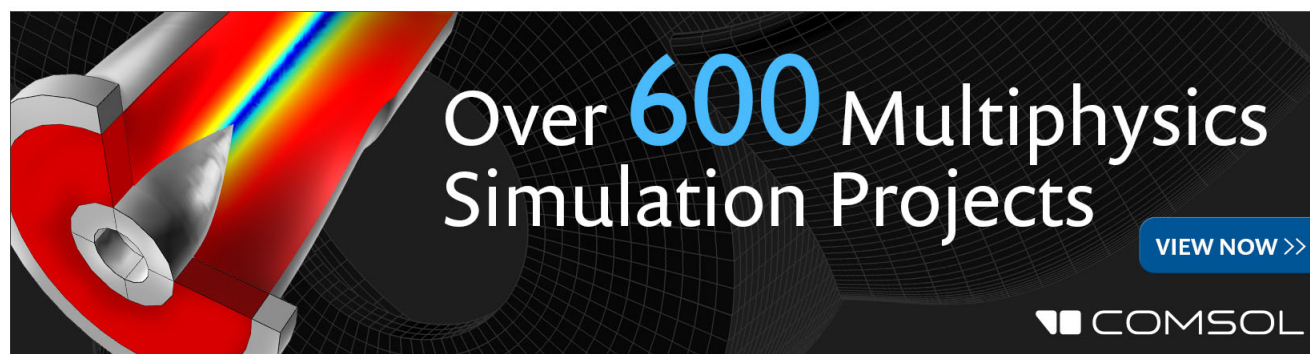
Appl. Phys. Lett. **98**, 044102 (2011); 10.1063/1.3545846

[A field evaporation deuterium ion source for neutron generators](#)

J. Appl. Phys. **103**, 094912 (2008); 10.1063/1.2913331

[Field evaporation behavior during irradiation with picosecond laser pulses](#)

Appl. Phys. Lett. **92**, 043503 (2008); 10.1063/1.2837626

The advertisement features a 3D simulation of a laser beam hitting a metal tip, with a color gradient from red to blue. The text 'Over 600 Multiphysics Simulation Projects' is prominently displayed in white and blue. A blue button with the text 'VIEW NOW >>' is located in the bottom right corner. The COMSOL logo is in the bottom right corner.

Over **600** Multiphysics Simulation Projects

[VIEW NOW >>](#)

COMSOL

Applicability of post-ionization theory to laser-assisted field evaporation of magnetite

D. K. Schreiber,^{1,a)} A. N. Chiaramonti,² L. M. Gordon,³ and K. Kruska⁴

¹Energy and Environment Directorate, Pacific Northwest National Laboratory, P.O. Box 999, Richland, Washington 99352, USA

²Material Measurement Laboratory, National Institute of Standards and Technology, 325 Broadway Str., Boulder, Colorado 80305, USA

³Environmental Molecular Sciences Laboratory, Pacific Northwest National Laboratory, P.O. Box 999, Richland, Washington 99352, USA

⁴Fundamental and Computational Science Directorate, Pacific Northwest National Laboratory, P.O. Box 999, Richland, Washington 99352, USA

(Received 30 September 2014; accepted 6 December 2014; published online 18 December 2014)

Analysis of the detected Fe ion charge states from laser-assisted field evaporation of magnetite (Fe_3O_4) reveals unexpected trends as a function of laser pulse energy that break from conventional post-ionization theory for metals. For Fe ions evaporated from magnetite, the effects of post-ionization are partially offset by the increased prevalence of direct evaporation into higher charge states with increasing laser pulse energy. Therefore, the final charge state is related to both the field strength and the laser pulse energy, despite those variables themselves being intertwined when analyzing at a constant detection rate. Comparison of data collected at different base temperatures also shows that the increased prevalence of Fe^{2+} at higher laser energies is possibly not a direct thermal effect. Conversely, the ratio of $^{16}\text{O}^+$:($^{16}\text{O}_2^+ + ^{16}\text{O}^+$) is well correlated with field strength and unaffected by laser pulse energy on its own, making it a better overall indicator of the field evaporation conditions. Plotting the normalized field strength versus laser pulse energy also elucidates a non-linear dependence, in agreement with the previous observations on semiconductors, which suggests field-dependent laser absorption efficiency. Together these observations demonstrate that the field evaporation process for laser-pulsed oxides exhibits fundamental differences from metallic specimens that cannot be completely explained by post-ionization theory. Further theoretical studies, combined with detailed analytical observations, are required to understand fully the field evaporation process of non-metallic samples. © 2014 AIP Publishing LLC.

[<http://dx.doi.org/10.1063/1.4904802>]

The commonplace analysis of non-metallic materials by atom probe tomography (APT) is a relatively new development made possible by the widespread availability of pulsed laser APT systems.^{1–3} Many questions persist about the field evaporation process of non-metallic specimens⁴ and the interaction between the nanoscopic APT specimen and the ultrafast lasers used to induce timed field evaporation.⁵ Recent studies^{6,7} have demonstrated that the band structure of dielectric and semiconducting specimens is altered by the intense electric field surrounding the APT specimen, potentially reaching metallic-like behaviors. In light of this effect, many regard the laser-assisted field evaporation of ions from electrically insulating specimens to be quite similar to that of metals where thermal pulsing is believed to be the dominant evaporation mechanism.⁸

One widely accepted idea within field evaporation theory is that of post-ionization. Briefly, post-ionization involves the initial evaporation of an ion that is further ionized into a higher charge state by tunneling of electron(s) back to the tip. The probability for post-ionization is both field and material dependent, with a higher field resulting in a greater probability of post-ionization. Kingham derived

plots of the anticipated charge states as a function of field for many metals^{9,10} and experimental confirmation exists¹¹ for many metals and Si. Post-ionization theory has not, however, been explored in great detail with modern APT instruments and non-metallic specimens. Ionic materials, in particular, could present a unique complication since the atoms are strongly polarized within the crystal itself. The Kingham diagrams explicitly assume that initial evaporation occurs as a singly charged ion, while Kellogg noted¹² that this assumption may be violated at high laser energies even when analyzing covalently bonded Si. It is therefore of interest to evaluate the measured charge states for an Fe oxide (magnetite, Fe_3O_4) as a function of laser pulse energy, base temperature, and field strength in the context of post-ionization theory. Magnetite was chosen as a model oxide system for its consistent stoichiometry, its relevance as an oxidation/corrosion product,^{13,14} and its narrow band gap that makes it an interesting ionic but nearly metallic material for considering field evaporation effects.¹⁵

APT specimens were prepared by focused ion beam lift out and annular milling (2 kV Ga^+ cleanup)¹⁶ from mineralogical magnetite along the [111] direction. The crystal structure and orientation were confirmed by Laue backscatter X-ray diffraction. APT determined the chemical purity to be >99.9% Fe and O. APT analyses used a LEAP 4000 XSi³¹

^{a)}Author to whom correspondence should be addressed. Electronic mail: daniel.schreiber@pnnl.gov.

and a LEAP 4000 XHR (Cameca Instruments), hereafter referred to as the Si and HR tools, with identical UV lasers (250 kHz repetition rate, $\lambda = 355$ nm, and ≈ 12 ps pulse duration) and focusing optics. The HR tool has a reflectron lens, while the Si tool has a straight flight path. The nominal detection rates (0.3% or 0.003 detected ions/pulse and 0.45% on the HR and Si tools, respectively) were set for a similar evaporation rate (≈ 0.008 evaporated ions/pulse in the field of view). All data from both tools were collected from a single tip, negating potential tip-to-tip variability, and approximately 6×10^5 ions were collected at each condition, discarding the first 1×10^5 ions to allow tip equilibration. The effects of laser pulse energy (0.05 pJ/pulse to 40 pJ/pulse), detection rate (0.3%–0.9% on the HR tool), and base temperature (40–120 K on the Si tool) were explored. The base pressure of the HR tool was 1.6×10^{-9} Pa at 40 K and that of the Si tool was 9.6×10^{-9} Pa at 40 K and 1.0×10^{-8} Pa at 120 K. Data analyses were performed with IVAS v3.6.6 (Cameca Instruments). The Fe charge state fraction (Fe *CSF*) and O ionic fraction (O *IF*) are described by $CSF = Fe^{2+}/(Fe^{1+} + Fe^{2+})$ and $IF = O^{1+}/(O^{1+} + O_2^{1+})$. The counting error is described as $2\sigma = 2\sqrt{f_i(1-f_i)/N}$ (two times the standard deviation), where f_i is the calculated fraction and N is the total number of ions contributing to that fraction. Note that FeH^{1+} (more prevalent in the Si tool) was considered the same as Fe^{1+} . Although not discussed here, the measured O concentration across all parameter space was O deficient compared to the nominal oxide stoichiometry. Representative mass spectra can be found in supplementary material.¹⁷

The relationship between laser pulse energy and normalized field strength for magnetite is shown in Figure 1(a) at 40 K and 0.45% detection rate (Si tool), where the normalized field strength (F/F_0) is defined as $F/F_0 = V/V_0$, and F_0 and V_0 (7250 V) are established at the lowest laser pulse energy (0.1 pJ/pulse). The voltage rise for collecting each data point is added to V_0 sequentially (~ 15 V/measurement) and the uncertainty in voltage is estimated as ± 75 V for laser drift. The linear relationship between field strength and the natural logarithm of laser pulse energy is somewhat surprising since metals consistently show a direct linear relationship between field and laser pulse energy.^{8,18,19} The Fe *CSF* and the O *IF* are plotted versus normalized field strength in Fig. 1(b). The Fe *CSF* exhibits a parabolic relationship with field strength that is inconsistent with post-ionization theory. As field decreases (corresponding to an increase in laser pulse energy) from 1.0, the Fe *CSF* decreases by 2.1% from 0.94 to 0.92. As the field decreases further, this trend reverses and the Fe *CSF* increases. This conflicts with post-ionization theory that predicts a further decrease in Fe *CSF* with the decreasing field strength. Quantification of molecular dissociations events^{17,20,21} altered the Fe *CSF* by $\sim 0.05\%$ for 10M ion datasets at both 40 pJ/pulse and 1.2 pJ/pulse and can therefore be generally neglected. Conversely, the O *IF* follows a monotonically decreasing but non-linear response with decreasing field strength. Because laser pulse energy is a more accessible experimental parameter, it is used in place of normalized field in the following figures, but the relationship shown in Fig. 1(a) can approximate the corresponding changes in field strength.

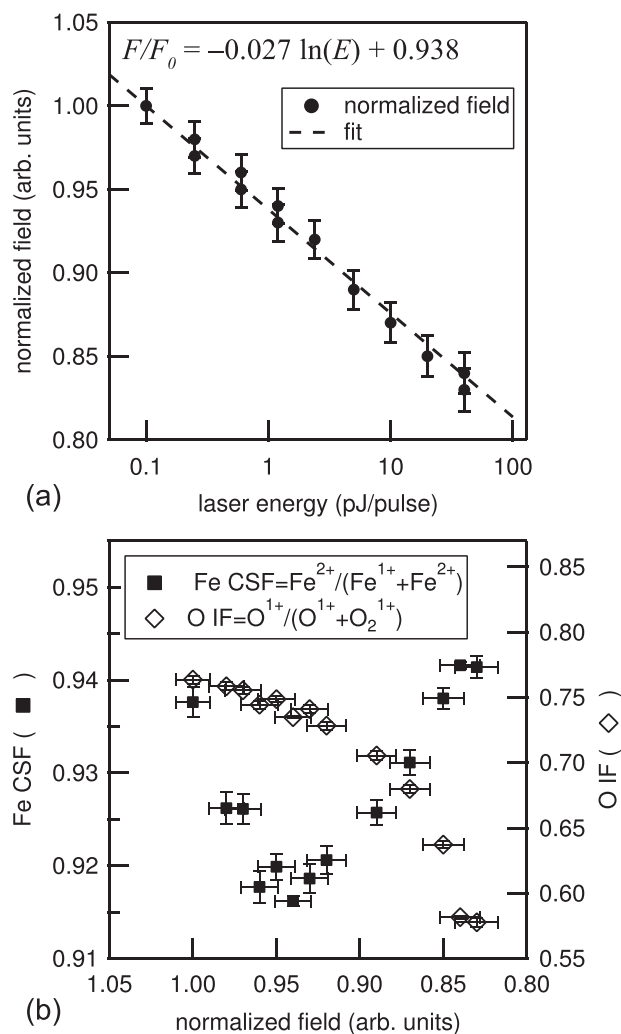


FIG. 1. Plots of (a) the normalized field strength (F/F_0) versus laser pulse energy (E) and (b) the mean Fe *CSF* (left axis) and ratio of O *IF* (right axis) as a function of the normalized field strength. (Si tool, 40 K and 0.45% detection rate.)

Measurements of the Fe *CSF* and O *IF* as a function of laser pulse energy at base temperatures of 40 K and 120 K (Si tool, 0.45% detection rate) and separately at detection rates of 0.3% and 0.9% (HR tool, 40 K) are shown in Figure 2. Increasing the base temperature depresses the Fe *CSF*, which is consistent with expectations from post-ionization theory as the field decreases to maintain the same evaporation rate. However, the trend for increasing Fe *CSF* with laser pulse energy persists at 120 K, and this is inconsistent with post-ionization theory. The effect of tripling the detection rate from 0.3% to 0.9%, thereby increasing the evaporation field by $\approx 3.5\%$, is confounded by the parabolic nature of the Fe *CSF*/laser pulse energy relationship. At laser pulse energies less than ≈ 20 pJ/pulse, the Fe *CSF* is higher at 0.9% than at 0.3% detection rate, while the opposite is true for laser energies greater than ≈ 20 pJ/pulse. This is counterintuitive with respect to post-ionization theory, wherein a higher standing field should universally generate a higher overall charge state. Instead, the minimum of the parabolic curve of the Fe *CSF* shifts to a higher laser pulse energy when the detection rate is increased causing the crossover at ≈ 20 pJ/pulse. Conversely, the O *IF* universally exhibits

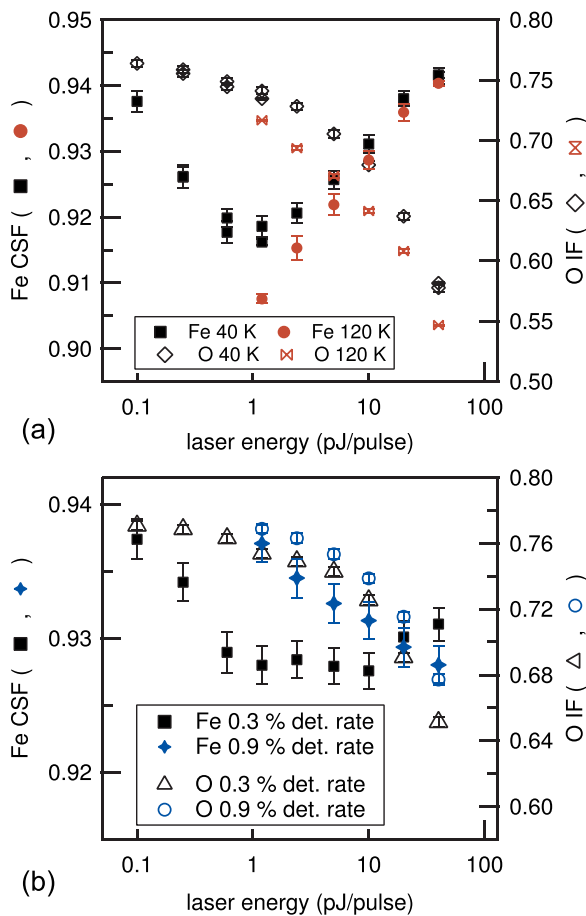


FIG. 2. (a) Plots of the Fe CSF (left axis) and the O IF (right axis) versus laser pulse energy at base temperatures of 40 K (black) and 120 K (red). Data from the Si tool at a detection rate of 0.45%. (b) Similar plots at detection rates of 0.3% and 0.9%. Data collected with the HR tool at a base temperature of 40 K.

field-dependent behaviors consistent with Fig. 1(b) of a higher fraction of O^{1+} at higher fields for both a higher detection rate and a lower base temperature.

Measurements at a fixed voltage and varied laser pulse energy delineate the effects of laser energy from field strength. The voltage (6670 V) was first established at a detection rate of 0.3% and 1.2 pJ/pulse and the laser pulse energy was increased to 2.4 pJ/pulse and then 5 pJ/pulse without changing the voltage (HR tool at 40 K), increasing the detection rate to $0.57 \pm 0.07\%$ and $1.18 \pm 0.12\%$, respectively. These data are plotted against data collected at a voltage-controlled, fixed 0.3% detection rate in Figures 3(a) and 3(b). If post-ionization dominated the Fe CSF, increasing the laser pulse energy at a fixed field strength would have a negligible effect on the measured Fe CSF. Such is the case for the O IF that is unchanged by increasing the laser pulse energy at a fixed field, but the Fe CSF instead increases with laser pulse energy. Therefore, it can be concluded that the O IF is primarily field dependent, while the Fe CSF is also directly correlated with laser pulse energy. With this in mind, the Fe CSF from Fig. 2(a) is replotted against the O IF at 40 K and 120 K. Assuming that the O IF is strictly field dependent, as suggested by Fig. 3(b), the O IF reflects the field strength (Fig. 1(b)) and can show indirectly the field-independent effect of base temperature on the Fe CSF. For a

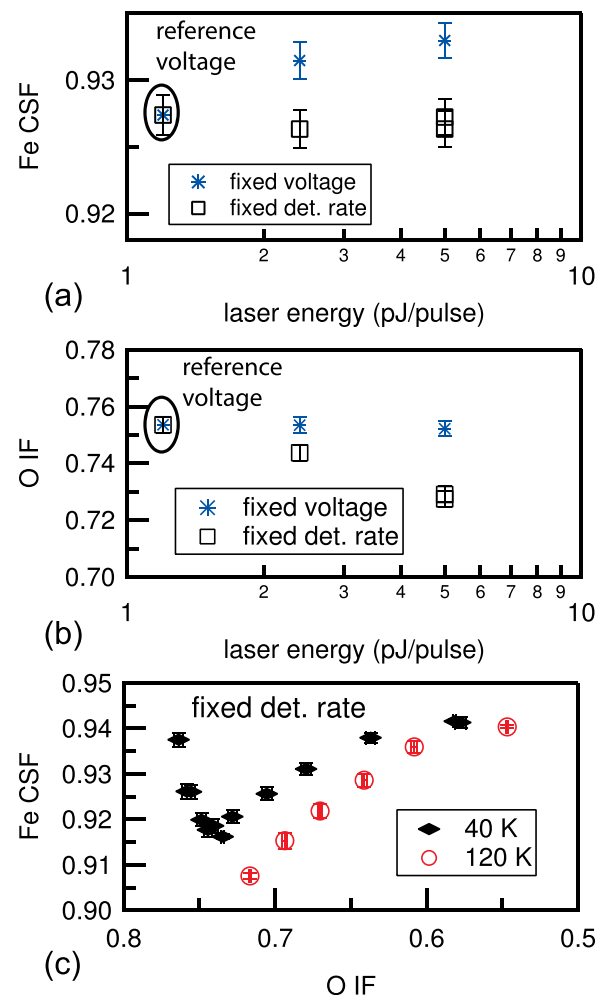


FIG. 3. Plots of (a) the Fe CSF and (b) the O IF with a voltage controlled, fixed detection rate (black squares) or with a fixed voltage (i.e., fixed evaporation field) and unrestricted detection rate (blue asterisk) as a function of laser pulse energy. The reference voltage was established at 1.2 pJ/pulse and 0.3% detection rate. Data collected with HR tool at a base temperature of 40 K. (c) Data from Fig. 2(a) replotted as Fe CSF versus O IF for 40 and 120 K and a fixed detection rate of 0.45%.

given O IF (i.e., field strength), the Fe CSF is universally lower at the higher base temperature. This is directly opposite the effect of increasing the laser energy at a fixed field strength, as shown in Fig. 3(a) in which a higher laser energy resulted in a higher Fe CSF. It can therefore be inferred that laser energy and base temperature have opposite effects on the Fe CSF in this parameter space.

Overall, the field evaporation of magnetite exhibits unanticipated features. First, the dependence of evaporation field on laser pulse energy shows an exponential relationship rather than the linear relationship documented for metallic specimens.^{8,18,19} It has been suggested that for semiconductors, this non-linearity is a result of increased laser absorption efficiency as the field strength increases, causing the surface temperature at a fixed laser intensity to increase with field strength.¹⁹ This explanation also seems plausible for magnetite, which is itself a narrow bandgap semiconductor,²² although more comprehensive studies as a function of temperature are needed to prove this outright. The local electrode geometry used here is not ideal to address temperature dependencies because the field enhancement factor is highly

sensitive to the specimen-to-electrode distance, which changes with temperature due to thermal expansion. While this can be partially compensated by repositioning the tip, more comprehensive temperature-field studies on nonmetals should instead use far-field electrode geometry tomographs. Nonetheless, the exponential field/laser pulse energy relationship shows a strong divergence from metallic field evaporation behavior.

Second, the Fe *CSF* for magnetite is not dictated exclusively by field-dependent post-ionization effects. Instead, it depends upon both post-ionization from singly charged to doubly charged Fe and direct evaporation as Fe^{2+} which becomes more energetically favorable at higher laser energies. Since these two trends are counter-indicated at a fixed detection rate, the resulting Fe *CSF* versus laser pulse energy can exhibit a parabolic relationship. Kellogg similarly observed the disappearance and reappearance of Si^{2+} as the field strength was decreased by increasing the laser pulse energy,¹² but this does not appear to have been documented previously for oxides.^{23,24} Note that image hump model predictions of the evaporation field strengths²⁵ for the dications Fe^{2+} and Si^{2+} are lower than those for Fe^{1+} and Si^{1+} , which could partially explain the observed trends in comparison to Mg and Zn oxides in which the dications evaporate at higher field strengths.²⁴ It is also shown that the laser energy dependence of the Fe *CSF* may not be a direct thermal effect. Increasing the base temperature from 40 K to 120 K depressed the Fe *CSF* for a given O *IF*, which is seemingly well-correlated with field strength, while increasing the laser energy at a fixed field strength unambiguously increased only the Fe *CSF*. More direct temperature-field studies could clarify this inferred correlation. Although not included here, we have made similar observations of the Fe *CSF* versus laser pulse energy, temperature, and detection rate for wüstite (Fe_{1-x}O) and hematite ($\alpha\text{-Fe}_2\text{O}_3$). Therefore, it is unlikely that these trends are unique to magnetite, which exhibits complicated phase changes at cryogenic temperatures,²² whereas wüstite and hematite do not.

In contrast to the Fe *CSF*, the O *IF* varied monotonically with field strength. Bachhav *et al.* also showed this for wüstite,²⁶ wherein they interpreted the peak at a mass-to-charge-state ratio of 16 Da as $^{16}\text{O}_2^{2+}$. This peak assignment is generally ambiguous between $^{16}\text{O}^+$ and $^{16}\text{O}_2^{2+}$ and its identification was sensible as the trends in the ratio of $\text{O}_2^{2+}:\text{O}_2^{1+}$ were consistent with post-ionization theory and also improved the overall oxide stoichiometry. However, subsequent studies^{27,28} using ^{18}O isotopic labelled $\alpha\text{-Fe}_2\text{O}_3$ and SiO_2 showed that the 16 Da peak is (within experimental error) exclusively $^{16}\text{O}^+$ and the observed trends were more likely of $\text{O}^{1+}:\text{O}_2^{1+}$, similar to the O *IF*, and are unrelated to post-ionization. Nonetheless, this ratio is a more reliable indicator of the field evaporation conditions than is the Fe *CSF*. Similarly, the $\text{O}^{1+}:\text{O}_2^{1+}$ ratio was a useful indicator of evaporation conditions for hydroxyapatite [$\text{Ca}_5(\text{PO}_4)_3(\text{OH})$] where the cations were observed with only a single charge state.²⁹ Little attention has been given to the field dependence of molecular ion formation through experiments³⁰ or modeling.⁶ Considering the consistent field dependence of the O *IF*, further attention should be given for understanding molecular ion evaporation and its potential as a metric for

reproducible analysis conditions in materials that exhibit molecular ion formation.

In summary, the charge states of Fe and the ionic fraction of O to O_2 species have been systematically analyzed as a function of laser pulse energy, field strength, base temperature, and detection rate. The Fe *CSF* varied with both laser pulse energy and field strength due to a competition between post-ionization at higher field strengths and direct evaporation into higher charge states at higher laser energies. Conversely, the O *IF* varied consistently with field strength and is a more reliable metric of the field evaporation conditions. Finally, the normalized field strength varied with the natural logarithm of laser pulse energy rather than the linear relationship observed for metallic specimens.

D.K.S. acknowledges funding from the U.S. Department of Energy (DOE) Office of Basic Energy Science and L.M.G. from the EMSL William Wiley Postdoctoral Fellowship. Sample preparation and LEAP 4000 XHR analyses were performed using EMSL, a national scientific user facility sponsored by DOE's Office of Biological and Environmental Research and located at Pacific Northwest National Laboratory (PNNL). PNNL is operated by Battelle for DOE under Contract No. DE-AC05-76RL01830.

¹K. Hono, T. Ohkubo, Y. M. Chen, M. Kodzuka, K. Oh-ishi, H. Sepehri-Amin, F. Li, T. Kinno, S. Tomiya, and Y. Kanitani, *Ultramicroscopy* **111**(6), 576–583 (2011).

²J. H. Bunton, J. D. Olson, D. R. Lenz, and T. E. Kelly, *Microsc. Microanal.* **13**(6), 418–427 (2007).

³B. Gault, F. Vurpillot, A. Vella, M. Gilbert, A. Menand, D. Blavette, and B. Deconihout, *Rev. Sci. Instrum.* **77**(4), 043705 (2006).

⁴E. P. Silaeva, M. Karahka, and H. J. Kreuzer, *Curr. Opin. Solid State Mater. Sci.* **17**(5), 211–216 (2013).

⁵T. F. Kelly, A. Vella, J. H. Bunton, J. Houard, E. P. Silaeva, J. Bogdanowicz, and W. Vandervorst, *Curr. Opin. Solid State Mater. Sci.* **18**(2), 81–89 (2014).

⁶M. Karahka and H. J. Kreuzer, *Ultramicroscopy* **132**, 54–59 (2013).

⁷E. P. Silaeva, N. S. Shcheblanov, T. E. Itina, A. Vella, J. Houard, N. Sevelin-Radiguet, F. Vurpillot, and B. Deconihout, *Appl. Phys. A* **110**(3), 703–707 (2013).

⁸A. Cerezo, G. D. W. Smith, and P. H. Clifton, *Appl. Phys. Lett.* **88**(15), 154103 (2006).

⁹R. Haydock and D. R. Kingham, *Phys. Rev. Lett.* **44**(23), 1520–1523 (1980).

¹⁰D. R. Kingham, *Surf. Sci.* **116**(2), 273–301 (1982).

¹¹G. L. Kellogg, *Surf. Sci.* **120**(2), 319–333 (1982).

¹²G. L. Kellogg, *Appl. Surf. Sci.* **11–12**, 186–195 (1982).

¹³K. Kruska, S. Lozano-Perez, D. W. Saxey, T. Terachi, T. Yamada, and G. D. W. Smith, *Corros. Sci.* **63**, 225–233 (2012).

¹⁴L. E. Thomas and S. M. Bruemmer, *Corrosion* **56**(6), 572–587 (2000).

¹⁵K. R. Kuhlman, R. L. Martens, T. F. Kelly, N. D. Evans, and M. K. Miller, *Ultramicroscopy* **89**(1–3), 169–176 (2001).

¹⁶K. Thompson, D. Lawrence, D. J. Larson, J. D. Olson, T. F. Kelly, and B. Gorman, *Ultramicroscopy* **107**(2–3), 131–139 (2007).

¹⁷See supplementary material at <http://dx.doi.org/10.1063/1.4904802> for representative APT mass spectra and quantification of molecular dissociations from Fe_3O_4 .

¹⁸F. Vurpillot, B. Gault, A. Vella, M. Bouet, and B. Deconihout, *Appl. Phys. Lett.* **88**(9), 094105 (2006).

¹⁹E. P. Silaeva, A. Vella, N. Sevelin-Radiguet, G. Martel, B. Deconihout, and T. E. Itina, *New J. Phys.* **14**, 113026 (2012).

²⁰D. W. Saxey, *Ultramicroscopy* **111**(6), 473–479 (2011).

²¹D. Santhanagopalan, D. K. Schreiber, D. E. Perea, R. L. Martens, Y. Janssen, P. Khalifah, and Y. S. Meng, *Ultramicroscopy* **148**, 57–66 (2015).

²²P. A. Miles, W. B. Westphal, and A. Vonhippel, *Rev. Mod. Phys.* **29**(3), 279–307 (1957).

²³E. P. Silaeva, L. Arnoldi, M. L. Karahka, B. Deconihout, A. Menand, H. J. Kreuzer, and A. Vella, *Nano Lett.* **14**(11), 6066–6072 (2014).

- ²⁴L. Mancini, N. Amirifar, D. Shinde, I. Blum, M. Gilbert, A. Vella, F. Vurpillot, W. Lefebvre, R. Lardé, E. Talbot, P. Pareige, X. Portier, A. Ziani, C. Davesne, C. Durand, J. Eymery, R. Butte, J.-F. Carlin, N. Grandjean, and L. Rigutti, *J. Phys. Chem. C* **118**, 24136 (2014).
- ²⁵B. Gault, M. P. Moody, J. M. Cairney, and S. P. Ringer, *Atom Probe Microscopy* (Springer, New York, NY, 2012).
- ²⁶M. Bachhav, R. Danoix, F. Danoix, B. Hannoyer, S. Ogale, and F. Vurpillot, *Ultramicroscopy* **111**(6), 584–588 (2011).
- ²⁷M. Bachhav, F. Danoix, B. Hannoyer, J. M. Bassat, and R. Danoix, *Int. J. Mass Spectrom.* **335**, 57–60 (2013).
- ²⁸T. Kinno, M. Tomita, T. Ohkubo, S. Takeno, and K. Hono, *Appl. Surf. Sci.* **290**, 194–198 (2014).
- ²⁹L. M. Gordon, L. Tran, and D. Joester, *ACS Nano* **6**(12), 10667–10675 (2012).
- ³⁰R. Kirchhofer, M. C. Teague, and B. P. Gorman, *J. Nucl. Mater.* **436**(1–3), 23–28 (2013).
- ³¹Commercial equipment, instruments, or materials are identified only in order to adequately specify certain procedures. In no case does such identification imply recommendation or endorsement by the National Institute of Standards and Technology nor does it imply that the products identified are necessarily the best available for the purpose.